On the relative importance of global and squirt flow in cracked porous media

Aamir Ali[1] and Morten Jakobsen[1, 2]

[1]*Department of Earth Sciences, University of Bergen, Allegaten 41, 5007 Bergen, Norway.*

[2]*Centre for Integrated Petroleum Research, University of Bergen, Allegaten 41, 5007 Bergen, Norway.*

Summary

A unified theory of global and squirt flow in cracked porous media was developed several years ago on the basis of a combination of the dynamic T-matrix approach to rock physics. The theory has been successfully used to model ultrasonic velocity and attenuation anisotropy measurements in real rocks under pressure. At the same time, it was recently pointed out that this theory, which contain an established theory of interconnected cracks as a special case contains an error related to fluid mass conservation. The error was recently corrected, and this paper represents an attempt to perform a systematic study of the implications of unified theory for the relative importance of global and squirt flow in cracked porous media characterized by different microstructures and fluid mobilities. Our numerical results suggest that squirt flow dominates over global flow and global flow appears to be more important at higher frequencies for more realistic models of microstructure. The attenuation peak of squirt flow move towards lower frequencies with the increasing fluid viscosity i.e. changing saturating fluid from water to oil, while the global flow attenuation peak move towards higher frequencies with increasing fluid viscosity. A previous observation of negative velocity dispersion in unified theory still remain, even if we use the correct

effective wave number, when dealing with the phenomenon of wave-induced fluid flow in models of cracked porous media where global flow effects dominates. The attenuation peak of the global flow obtained using the correct wave number is always shifted to the left as compared to the approximate solution. At seismic frequencies global flow effects are not so important and needs very high permeability and low viscosity to have an effect.

Keywords: Wave induced fluid flow, Attenuation, Velocity dispersion, Cracked porous media

1 Introduction

In seismic modelling, a cracked porous medium can sometimes be replaced by a long wavelength equivalent homogenous medium that can be both anisotropic and viscoelastic due to microstructural alignments and wave induced fluid flow, respectively. Wave induced fluid flow can occur in the form of global or squirt flow. Global flow is caused by pressure gradients at the scale of the acoustic wavelength and in the direction of wave propagation, whereas squirt flow is caused by the pressure gradients at the microscopic or mesoscopic scale and in directions that are potentially different from that of the wave propagation. There have been several attempts to develop special (phenomenological or microstructural) theories of global flow (Biot 1962; Hudson *et al*. 1996), special (microstructural) theories of squirt flow (Mavko and Nur 1975; O'Connell and Budiansky 1977; Mavko and Jizba 1991; Mukerji and Mavko 1994; Dvorkin *et al*. 1995; Chapman 2003), and unified (phenomenological and microstructural) theories of global and squirt flow (Dvorkin and Nur 1993; Hudson *et al*. 1996; Chapman *et al*. 2002; Jakobsen *et al*. 2003b; Jakobsen 2004).

The unified theory of Jakobsen *et al*. (2003b), which contains the theory of interconnected cracks developed by Hudson *et al*. (1996) as a special case, originally had an error related to fluid mass conservation, but this error was recently corrected by Jakobsen and

Chapman (2009). Unlike the unified theory of Chapman *et al*. (2002), the corrected version of the theory of Jakobsen *et al*. (2003b) presented by Jakobsen and Chapman (2009) can deal with effects of anisotropy as well as attenuation.

In the unified theories for global and squirt flow presented by Hudson *et al*. (1996), Jakobsen *et al*. (2003b) and Jakobsen and Chapman (2009), the effective stiffness tensor $\mathbf{C}^*$ depends on the effective wave vector $\mathbf{k}^*$ and as well as on the angular frequency ω. Since we are dealing with theories of the coupled physical process of wave-induced fluid flow, this is perhaps not surprising. In all previous studies, these non-local effects have been avoided simply by replacing the effective wave vector $\mathbf{k}^*$ by the unperturbed wave vector $\mathbf{k}$ associated with the waves in the solid reference medium; that is, by using the approximation $k^* \approx k = \omega / V^{(0)}$, where ω is the angular frequency, $V^{(0)}$ is the speed of the wave mode under consideration in the solid matrix and k is the length of $\mathbf{k}$. This approximation for effective wave vector $\mathbf{k}^*$ was considered to be one of the possible explanations for predictions of negative velocity dispersion in numerical experiments dealing with the phenomenon of wave-induced fluid flow in models of cracked porous media where global flow effects dominates (Jakobsen and Chapman 2009).

An important aim of this study is to investigate the implications of unified theory of Jakobsen and Chapman (2009) for the relative importance of global and squirt flow characterized by different microstructures and fluid mobilities. A change in the viscosity may lead to a shift of the attenuation peak towards lower or higher frequencies, depending on the mechanism of wave-induced fluid flow. The influence of viscosity on attenuation peaks of the global and squirt flow is different depending on the type of mechanism involved (Xi *et al*. 2007). Also the experimental observations show that the high fluid viscosity can act to shift the relaxation towards lower frequencies (Winkler *et* al. 1985; Dvorkin *et al*. 1994). So it will

be very interesting to investigate the effects of viscosity in the context of relative importance of global and squirt flow.

A further aim is to investigate if this velocity dispersion will remain negative in these models, if we use the effective wave vector $\mathbf{k}^*$ rather than the unperturbed wave vector **k**; that is, if we implement the global flow part of the theory in a proper manner.

We use an iterative method for solving the nonlinear equations associated with the unified theory of global and squirt flow in cracked porous media, where the effective stiffness tensor depends on the frequency ω and effective wave vector $\mathbf{k}^*$. A quadratic equation representing microstructural and phenomenological theories of wave-induced fluid flow in isotropic media to the first order in porosity and crack density is also presented. We also present and apply a simple model for the effects of viscosity on the relaxation time constant for squirt flow associated with a particular pore shape/orientation.

2 Unified theory of global and squirt flow in cracked porous media

We consider a model in which a solid contains inclusions or cavities characterized by different shapes, orientations and spatial distributions labeled by $n = 1,...,N$. The effective stiffness tensor $\mathbf{C}^*$ is given by Jakobsen *et al*. (2003a, b),

$$\mathbf{C}^* = \mathbf{C}^{(0)} + \mathbf{C}_1 : (\mathbf{I}_4 + \mathbf{C}_1^{-1} : \mathbf{C}_2)^{-1}, \tag{1}$$

where

$$\mathbf{C}_1 = \sum_{r=1}^{N} v^{(r)} \mathbf{t}^{(r)}, \tag{2}$$

and

$$\mathbf{C}_2 = \sum_{r=1}^{N} \sum_{s=1}^{N} v^{(r)} \mathbf{t}^{(r)} : \mathbf{G}_d^{(rs)} : \mathbf{t}^{(s)} v^{(s)}. \tag{3}$$

Here $\mathbf{C}^{(0)}$ represents the elastic properties of the solid matrix, : denotes the double scalar product (see Auld 1990), $\mathbf{I}_4$ is the (symmetric) identity for fourth-rank tensors and $\mathbf{G}_d^{(rs)}$ is given by the strain Green's function integrated over an ellipsoid having the same aspect ratio

as $p^{(s|r)}(\mathbf{x}-\mathbf{x}')$, which in turn gives the probability density for finding an inclusion of type s at $\mathbf{x}'$, given that there is an inclusion of type r at point $\mathbf{x}$ (Jakobsen *et al*. 2003a, b). The t-matrix for an inclusion of type r fully saturated with a homogenous fluid is given by (Jakobsen and Chapman 2009)

$$\mathbf{t}^{(r)} = \mathbf{t}_d^{(r)} + \mathbf{t}_d^{(r)} : \mathbf{S}^{(0)} : (\mathbf{I}_2 \otimes \boldsymbol{\psi}^{(r)}) : \mathbf{C}^{(0)}, \tag{4}$$

and

$$\mathbf{t}_d^{(r)} = -\mathbf{C}^{(0)} : (\mathbf{I}_4 + \mathbf{G}^{(r)} : \mathbf{C}^{(0)})^{-1}. \tag{5}$$

Here, $\mathbf{S}^{(0)} = (\mathbf{C}^{(0)})^{-1}$ is the compliance tensor of the solid matrix material; $\mathbf{I}_2$ is the identity tensor for second-rank tensors; $\otimes$ is the dyadic tensor product (see Jakobsen *et al*. 2003a, b), $\mathbf{G}^{(r)}$ is a fourth-rank tensor given by the strain Green's function (for a material with properties given by $\mathbf{C}^{(0)}$) integrated over a characteristic spheroid having the same shape as cavities of type r (Jakobsen and Chapman 2009) and $\boldsymbol{\psi}^{(r)}$ is a second-rank tensor (fluid polarization tensor) that relates the fluid pressure to the applied stress. The fluid polarization tensor $\boldsymbol{\psi}^{(r)}$ is given by Jakobsen and Chapman (2009) under the assumption that the cavities are of the same scale-size and the squirt flow relaxation constant τ is independent of the shape and orientation. The analysis of Chapman *et al*. (2002) suggests that τ depends on the scale-size of the cavity, suggesting that the theory can easily be extended to model the cracked/fractured porous media under the assumption of inclusions or cavities of type r having different sizes. After letting the τ having an index r dependent on scale-size of the cavities the $\boldsymbol{\psi}$-tensor has the form

$$\boldsymbol{\psi}^{(r)} = \frac{-\widetilde{\boldsymbol{\Theta}}\sum_r \dfrac{\phi^{(r)}\mathbf{I}_2 : \mathbf{K}_d^{(r)}}{1+i\omega\gamma^{(r)}\tau^{(r)}} - i\omega\tau^{(r)}\kappa_f \mathbf{I}_2 : \mathbf{K}_d^{(r)}}{1+i\omega\gamma^{(r)}\tau^{(r)}}, \tag{6}$$

where,

$$\gamma^{(r)} = 1 + \kappa_f \mathbf{I}_2 : (\mathbf{K}_d^{(r)} - \mathbf{S}^{(0)}) : \mathbf{I}_2, \tag{7}$$

$$\mathbf{K}_d^{(r)} = (\mathbf{I}_4 + \mathbf{G}^{(r)}\mathbf{C}^{(0)})^{-1} : \mathbf{S}^{(0)}, \tag{8}$$

$$\widetilde{\mathbf{\Theta}} = \kappa_f \left[\sum_r \frac{\phi^{(r)}\gamma^{(r)}}{1 + i\omega\gamma^{(r)}\tau^{(r)}} - \frac{iK_{ij}^* k_i^* k_j^* \kappa_f}{\eta_f \omega (1 - \Delta^{(r)})} \right]^{-1}, \tag{9}$$

and

$$\Delta^{(r)} = \frac{K_{ij}^* k_i^* k_j^* \kappa_f}{\phi \eta_f} \tau^{(r)}. \tag{10}$$

Here K_{ij}^* are the components of the effective permeability tensor of the cracked/fractured porous media and k_i^* represents the component of the effective wave number vector, where $i, j = 1,2,3$, κ_f is the bulk modulus for the fluid, η_f is the viscosity of the fluid, ϕ is the total porosity and ω is the angular frequency of the wave, respectively.

For the case of anisotropic media, the real-valued phase velocities and attenuation factors can be obtained by inserting the viscoelastic effective stiffness tensor $\mathbf{C}^*$ into the Christoffel equation (see Appendix-A), which can be solved by using eigenvalue/eigenvector method (Jakobsen *et al*. 2003b; Carcione 2007). The phase velocity is the reciprocal of the slowness and is given in the component form by (Carcione 1995, 2007)

$$\mathbf{V}_p = \left(\mathrm{Re}\left[\frac{1}{V} \right] \right)^{-1} \hat{\mathbf{I}}. \tag{11}$$

The quality factor Q is defined as the ratio of the peak strain energy to the average loss energy density (Auld 1990), and is defined by (Carcione 1995, 2007)

$$Q = \frac{\mathrm{Re}(V^2)}{\mathrm{Im}(V^2)}. \tag{12}$$

3 Exact analytical solution of wave-induced fluid-flow in isotropic models with randomly oriented ellipsoids

In this section, we derive exact analytical solution for a model of randomly oriented ellipsoids to the first order in porosity or crack density. We start from the relation of effective stiffness to the first order in porosity or crack density

$$\mathbf{C}^* = \mathbf{C}^{(0)} + \varphi \bar{\mathbf{t}}, \tag{13}$$

where φ is the porosity and $\bar{\mathbf{t}}$ is the averaged t-matrix for a single communicating cavity. Using equation (55) from Jakobsen *et al*. (2003b) for the averaged t-matrix with modified term $\widetilde{\mathbf{\Theta}}$ from Jakobsen and Chapman (2009) in order to account for global flow in a consistent manner and substituting in equation (13), we get

$$\mathbf{C}^* = \mathbf{C}^{(0)} + \varphi \left(\bar{\mathbf{t}}_d + \frac{\widetilde{\mathbf{\Theta}} \overline{\mathbf{Z}} + i\omega\tau\kappa_f \overline{\mathbf{X}}}{1 + i\omega\gamma\tau} \right). \tag{14}$$

Here, ω is the angular frequency, κ_f is the bulk modulus for fluid and τ is the squirt flow relaxation time. The relations for $\overline{\mathbf{Z}}$, and $\overline{\mathbf{X}}$ are given and discussed in detail by Jakobsen *et al* (2003b). We now have

$$\mathbf{C}^* = \mathbf{C}^{*d} + \varphi \left(\frac{\widetilde{\mathbf{\Theta}} \overline{\mathbf{Z}} + i\omega\tau\kappa_f \overline{\mathbf{X}}}{1 + i\omega\gamma\tau} \right), \tag{15}$$

where

$$\mathbf{C}^{*d} = \mathbf{C}^{(0)} + \varphi \bar{\mathbf{t}}_d \,. \tag{16}$$

The relation for velocity in terms of stiffness for an isotropic medium is given by

$$V = \sqrt{\frac{C_{11}^*}{\rho}}, \qquad \text{or} \qquad C_{11}^* = \rho V^2 . \tag{17}$$

Equation (15) can be written as,

$$C_{11}^* = C_{11}^{*d} + \varphi \left(\frac{\widetilde{\mathbf{\Theta}} \overline{Z}_{11} + i\omega\tau\kappa_f \overline{X}_{11}}{1 + i\omega\gamma\tau} \right). \tag{18}$$

The relation for modified term $\tilde{\Theta}$ is given by (Jakobsen and Chapman, 2009)

$$\tilde{\Theta} = \kappa_f \left[\sum_{r=1}^{N} \frac{\varphi^{(r)} \gamma^{(r)}}{1 + i\omega\gamma^{(r)}\tau} - \frac{i\kappa_f K_{ij} k_i k_j}{\eta_f \omega(1-\Delta)} \right]^{-1}, \tag{19}$$

where

$$\Delta = \frac{\kappa_f \tau}{\phi \eta_f} K_{ij} k_i k_j . \tag{20}$$

Substituting Δ in relation for $\tilde{\Theta}$ (equation (19)) and simplifying by using the relation for the wave-number as following

$$V = \frac{\omega}{k} \Rightarrow k = \frac{\omega}{V} \Rightarrow k = \frac{\omega}{\sqrt{\frac{C_{11}^*}{\rho}}} \Rightarrow k^2 = \frac{\omega^2 \rho}{C_{11}^*}. \tag{21}$$

After simplification and re-arranging we are left with a simple quadratic equation in C_{11}^* written as

$$\begin{aligned} &C_{11}^{*\,2}\left(\eta_f \varphi\gamma + i\omega\gamma^2 \tau\eta_f \varphi\right) + C_{11}^*(\kappa_f K_{ij}\omega^2 \rho\gamma\tau - i\kappa_f K_{ij}\omega\rho - C_{11}^{*d}\eta_f \varphi\gamma - iC_{11}^{*d}\omega\gamma^2\tau\eta_f\varphi \\ &- \kappa_f \eta_f \varphi \bar{Z}_{11} - i\eta_f \omega\gamma\tau\kappa_f \varphi \bar{Z}_{11} - i\omega\tau\kappa_f \bar{X}_{11}\varphi^2\gamma\eta_f) + iC_{11}^{*d}\kappa_f K_{ij}\omega\rho - C_{11}^{*d}\kappa_f K_{ij}\omega^2\rho\gamma\tau \\ &+ \kappa_f^2 \tau K_{ij}\omega^2\rho\bar{Z}_{11} + i\omega^3\gamma\tau^2\kappa_f^2 K_{ij}\rho\bar{Z}_{11} - \omega^2\tau\kappa_f^2 \bar{X}_{11}\varphi K_{ij}\rho = 0. \end{aligned} \tag{22}$$

Using equation (17) and representing equation (22) in terms of velocity V, we have

$$\left(V^2\right)^2 A + V^2 B + C = 0, \tag{23}$$

where

$$\begin{aligned} A &= \rho\eta_f \varphi\gamma + i\rho\omega\gamma^2\tau\eta_f\varphi, \\ B &= \kappa_f K_{ij}\omega^2\rho\gamma\tau - i\kappa_f K_{ij}\omega\rho - C_{11}^{*d}\eta_f\varphi\gamma - iC_{11}^{*d}\omega\gamma^2\tau\eta_f\varphi - \kappa_f\eta_f\varphi\bar{Z}_{11} \\ &- i\eta_f\omega\gamma\tau\kappa_f\varphi\bar{Z}_{11} - i\omega\tau\kappa_f\bar{X}_{11}\varphi^2\gamma\eta_f, \\ C &= iC_{11}^{*d}\kappa_f K_{ij}\omega - C_{11}^{*d}\kappa_f K_{ij}\omega^2\gamma\tau + \kappa_f^2\tau K_{ij}\omega^2\bar{Z}_{11} + i\omega^3\gamma\tau^2\kappa_f^2 K_{ij}\bar{Z}_{11} \\ &- \omega^2\tau\kappa_f^2\bar{X}_{11}\phi K_{ij}. \end{aligned} \tag{24}$$

Equation (24) is a quadratic equation which can be solved by a quadratic formula giving two solutions. The first solution is for the fast P-wave mode and the second solution is

slow P-wave mode (Biot 1956). We have only used the solution for the fast P-wave mode in our numerical experiments. The analysis for the slow P-wave mode is beyond the scope of this study and will be addressed in another paper.

4 Numerical Experiments

In this section, we report from numerical experiments dealing with the effect related with different microstructures and fluid mobilities on the relative importance of global and squirt flow in cracked/fractured porous media. The exact analytical solution derived in section 3 is limited to isotropic models of solids with randomly oriented ellipsoids to the first order in porosity or crack density. We have also used the iterative method for solving the nonlinear equations associated with the unified theory of global and squirt flow in cracked porous media, where the effective stiffness tensor depends on the frequency ω and effective wave vector $\mathbf{k}^*$. The starting point of the iterations is being the wave-number associated with the waves in the solid reference medium. The iterative solution is important to implement the global flow part correctly, when investigating the relative importance of global and squirt flow in complex microstructural models and to the higher order in porosity and crack density.

For the background elastic properties, we take $\kappa = 37$ GPa, $\mu = 44$ GPa, and $\rho = 2.5$ g/cm^3 to simulate the properties of quartz. The characteristic time scale constant or squirt flow relaxation time for micro-porosity (pores and micro-cracks) with water as a saturating fluid was taken to be $\tau_w = 10^{-5}$ s. We have applied a simple model for the effects of viscosity on the relaxation time constant for squirt flow associated with a particular pore shape/orientation (also see Chapman 2001). The squirt flow relaxation time for other fluids (oil or gas) can be calculated using the relation:

$$\tau = \eta\left(\frac{\tau_w}{\eta_w}\right), \tag{25}$$

where τ and η are the relaxation time and viscosity of the corresponding fluid (can be oil of gas), while η_w is the viscosity of water. The viscosity of water, oil and gas is 10^{-3} Pa s, 3×10^{-3} Pa s and 2×10^{-5} Pa s, respectively (see Pointer *et al*. 2000).

4.1 Isotropic models

Spherical pores

To investigate the relative importance of global and squirt flow for a simple model of spherical pores, we have divided the analysis in three numerical examples. The comparison for each example is presented in the form of T-matrix estimates of velocity and attenuation spectra of the plane wave propagation for different fluid mobilities.

In the first example (Fig. 1), we compare the exact, iterative and approximate solutions (the approximation for the wave-number $k^* \approx k = \omega / V^{(0)}$) to the first-order in porosity. The T-matrix estimates are obtained using the first-order T-matrix approach.

The second example (Fig. 2) is same as example 1, but for higher porosity. The T-matrix estimates obtained in this example may not be strictly valid at higher porosities, but the purpose is to investigate the performance of exact analytical solution.

The third example (Fig. 3) deals with the comparison of only iterative and approximate solutions for higher porosity. The T-matrix estimates are obtained using the higher-order T-matrix approach with a spherically symmetric correlation function.

For a model of spherical pores, there is no dependence on the characteristic time for squirt flow, because no local pressure gradients exist for such kind of a model. We only observe global flow in all the three examples (Figs. 1, 2 and 3) characterized by negative dispersion at higher frequencies, when the porous rock model is considered to be fully saturated with water or oil. No global flow is observed in the case when the porous rock model is considered to be fully saturated with gas (Figs. 1, 2 and 3). The attenuation peak for

global flow move towards relatively high frequencies when viscosity is increased for this particular model i.e. saturating fluid of the porous matrix is changed from water to oil (Figs. 1, 2 and 3). An increase in the matrix permeability from 1 to 10 Darcy shifts the global flow attenuation peak to relatively lower frequencies (Figs. 1, 2 and 3).

In the first example, the exact, iterative and approximate solutions clearly follow each other. Very small differences exist for the case of approximation with respect to the exact and iterative solution (Fig. 1). For the second example, observable differences exist in the case of approximation with respect to the exact and iterative solution (Fig. 2). The global flow attenuation peak of the approximate solution is shifted to right as compared to the exact and iterative solution (Fig. 2). Similarly in the third example, the global flow attenuation peak of the approximate solution is shifted to the right as compared to the iterative solution (Fig. 3).

Randomly oriented micro-cracks

The investigation of relative importance of global and squirt flow for a model of randomly oriented micro-cracks is also similarly divided in three numerical examples as for the case of spherical pores (Figs. 4, 5 and 6).

For a model consisting of randomly oriented micro-cracks, we observe squirt flow (positive dispersion) at lower frequencies due to different orientations of randomly oriented micro-cracks along with global flow (negative dispersion) at higher frequencies, when the porous rock model is considered to be fully saturated with water or oil (Figs. 4, 5 and 6). The squirt and global flow parts change their positions i.e. we observe global flow at lower frequencies and squirt flow at higher frequencies, when porous matrix is considered to be fully saturated with gas (Figs. 4, 5 and 6). The magnitude of global flow part dominates over the squirt flow part for this particular model (Figs. 4, 5 and 6). The attenuation peaks of global and squirt flow move towards relatively high and low frequencies when viscosity is increased for this particular model i.e. saturating fluid of the porous matrix is changed from water to oil

(Figs. 4, 5 and 6). The attenuation peak for the global flow part shifts toward relatively low frequencies when matrix permeability is increased from 1 Darcy to 10 Darcy (Figs. 4, 5 and 6).

The exact, iterative and approximate solutions clearly follow each other in the first numerical example. Very small differences exist for the case of approximation with respect to the exact and iterative solution only for the global flow part (Fig. 4). For the second example, observable differences exist in the case of approximation with respect to the exact and iterative solution only for the global flow part (Fig. 5). The global flow attenuation peak for the case of approximate solution is shifted to right as compared to the exact and iterative solution (Fig. 5). Similarly in the third example, the global flow attenuation peak of the approximate solution is shifted to the right as compared to the iterative solution (Fig. 6).

Spherical pores and randomly oriented micro-cracks

Fig. 7 shows the result of a comparison of the iterative and approximate solutions for a model of spherical pores and randomly oriented cracks in the form of T-matrix estimates (obtained using higher-order T-matrix approach with a spherically symmetric correlation function) of velocity and attenuation spectra of plane wave propagation to higher-order in porosity and crack density for different fluid mobilities. We observe both squirt and global flow with the dominance of squirt flow part for the case when the porous rock model is considered to be fully saturated with water or oil. The squirt flow for the case of the porous rock model saturated with water or oil is observed at relatively lower frequencies depending on the squirt flow relaxation time, while global flow is observed at relatively higher frequencies.

Only squirt flow is observed at relatively higher frequencies when the porous rock model is considered to be fully saturated with gas. The squirt and global flow attenuation peaks move towards relatively low and high frequencies, when viscosity is increased for this

particular model i.e. saturating fluid of the porous rock model is changed from water to oil. The global flow attenuation peak shifts toward relatively low frequencies when matrix permeability is increased from 1 to 10 Darcy.

Very small differences exist for the global flow part (Fig.7), and the global flow attenuation peak is shifted to the right for the case of approximate solution as compared to the iterative solution.

4.2 Anisotropic models

Aligned micro-cracks

Fig. 8 shows the result of a comparison of the iterative and approximate solutions for a model of aligned micro-cracks in the form of T-matrix estimates (obtained using higher-order T-matrix approach with correlation function equal to the aspect ratio of micro-cracks) of velocity and attenuation spectra of plane wave propagation to higher order in porosity and crack density for different fluid mobilities. Like in the case of spherical pores, there is no dependence on the characteristic time for squirt flow in this case, because no local pressure gradients exist for such kind of a model. We observe global flow characterized by negative dispersion at higher frequencies, when the porous rock model is considered to be fully saturated with water, oil or gas.

The magnitude of global flow is smaller, when the porous rock model is considered to be fully saturated with gas. The global flow attenuation peak move towards relatively high frequencies when viscosity is increased for this particular model i.e. saturating fluid of the porous rock model is changed from water to oil. An increase in matrix permeability from 1 to 10 Darcy shifts the global flow attenuation peak towards relatively lower frequencies.

Observable differences exist in the approximate solution with respect to iterative solution and the global flow attenuation peak is shifted towards the right for the approximate solution as compared to the iterative solution (Fig. 8).

Pores and aligned micro-cracks

Fig. 9 shows the result of a comparison of the iterative and approximate solutions for a model of pores and aligned micro-cracks in the form of T-matrix estimates (obtained using higher-order T-matrix approach with correlation function equal to the aspect ratio of micro-cracks) of velocity and attenuation spectra of plane wave propagation to higher-order in porosity and crack density for different fluid mobilities. We observe squirt and global flow at low and high frequencies with the dominance of squirt flow part the case when the porous rock model is considered to be fully saturated with water or oil (Fig. 9). We only observe squirt flow at higher frequencies when the porous rock model is considered to be fully saturated with gas.

The squirt and global flow attenuation peaks move towards relatively low and high frequencies, when viscosity is increased for this particular model i.e. saturating fluid of the porous rock model is changed from water to oil. The global flow attenuation peak shifts toward relatively low frequencies when matrix permeability is increased from 1 to 10 Darcy. Very small differences exist for the global flow part (Fig. 9) for the case of approximate solution as compared to the iterative solution.

Spherical pores, randomly oriented micro-cracks and aligned meso-fractures

We finally consider a more realistic model consisting of pores, randomly oriented cracks and one set of aligned meso-fractures. The orientation of meso-fractures is 45^{o}. For this case, the elastic background properties are $\kappa = 70\,\text{GPa}$, $\mu = 29\,\text{GPa}$, and $\rho = 2.71\,\text{g/cm}^3$ to simulate the properties of calcite. For aligned meso-fractures the characteristic time scale constant with water as the saturating fluid was calculated depending on the size/length of the fractures using the flowing relation (Chapman 2003, Agersborg *et al*. 2007)

$$\tau_f = \frac{r_f}{\xi}\tau_m . \tag{26}$$

Here, τ_f is the squirt flow relaxation time for the meso-fractures, r_f is the radius of fractures, ξ is the size of the grains (200×10^{-6} m assumed in this study) and τ_m is the squirt flow relaxation time for micro-porosity. The squirt flow relaxation times corresponding to different fluids (oil or gas) can be computed using equation (25). The characteristic time scale constant or squirt flow relaxation time for micro-porosity (pores and randomly oriented cracks) with water as a saturating fluid is taken to be $(\tau_m)_w = 2\times10^{-7}$ s. The radius of fractures in this study is 0.5 m.

In order to obtain the iterative solution for this particular case, effective permeability $\mathbf{K}^*$ along with the correct use of wave-number (effective wave-number $\mathbf{k}^*$) must be used, because two types of permeabilities exist in this model i.e. matrix permeability (due to pores and micro-cracks) and fracture permeability (due to aligned meso-fractures). This is also explained by the fact that the terms for effective permeability components (K_{ij}) and effective wave number components ($k_i k_j$) always come together in Jakobsen and Chapman (2009) theory indicating a summation over the indices $i, j = 1,2,3$ (see equation (9)). Their contraction can be written as by expanding the summation over indices and collecting the identical terms

$$K_{ij}k_i k_j = K_{11}k_1^2 + 2K_{12}k_1k_2 + 2K_{13}k_1k_3 + K_{22}k_2^2 + +2K_{23}k_2k_3 + K_{33}k_3^2 . \tag{27}$$

To obtain the independent effective permeability components for this particular model, we used the effective permeability model of Jakobsen (2007) (see appendix-B). The effective wave vector $\mathbf{k}^*$ is given by

$$\mathbf{k}^* = k^*\mathbf{l} \tag{28}$$

where k^* is the length of $\mathbf{k}^*$ and $\mathbf{l}$ in spherical coordinates is given by

$$\mathbf{l} = \begin{bmatrix} l_1 \\ l_2 \\ l_3 \end{bmatrix} = \begin{bmatrix} \sin\theta\sin\varphi \\ \sin\theta\cos\varphi \\ \cos\theta \end{bmatrix}. \tag{29}$$

Then the components of effective wave vector $\mathbf{k}^*$ are given by

$$\begin{aligned} k_1^* &= k^* l_1 \\ k_2^* &= k^* l_2 \\ k_3^* &= k^* l_3 \end{aligned} . \tag{30}$$

Fig. 10 shows the result of comparison of iterative and approximate solutions for a model of pores, randomly oriented cracks and meso-fractures in the form of T-matrix estimates (obtained using higher-order T-matrix approach with correlation function equal to the aspect ratio of meso-fractures) of velocity and attenuation spectra of plane wave propagation to higher order in porosity and fracture density for different mobilities. Approximate solution for this case was obtained by using approximation for wave-number as well as the matrix permeability instead of effective permeability.

Due to the introduction of one set of aligned meso-fractures, we observe squirt flow (positive dispersion) associated with aligned set of meso-fractures as well as due to micro-porosity (pores and micro-cracks). The squirt flow peak associated with the aligned mesoscopic fracture set is observed at seismic frequencies, while the squirt flow peak associated with micro-porosity (pores and randomly oriented cracks) is observed at higher frequencies, respectively, when the porous rock model is considered to be fully saturated with water or oil. We only observe squirt flow associated with meso-fractures and micro-porosity at higher frequencies, when the porous rock model is considered to be fully saturated with gas. Global flow characterized by negative dispersion is also observed at relatively higher frequencies, with water or oil as the saturating fluids in the porous rock model.

The attenuation peak for squirt and global flow move towards relatively low and high frequencies when viscosity is increased for this particular model i.e. saturating fluid of the porous rock model is changed from water to oil. The attenuation peak of the global flow shifts toward relatively lower frequencies when matrix permeability is increased from 1 to 10 Darcy.

Very small differences exist in the case of approximate solution as compared to iterative solution only for the global flow part. The global flow attenuation peak in the case of approximate solution is shifted to right as compared to the iterative solution (Fig. 10).

5 Conclusions

We have investigated the relative importance of global and squirt flow in cracked/fractured porous media using the unified theory (Jakobsen and Chapman, 2009) for different microstructures and fluid mobilities. The magnitude of squirt flow dominates over global flow and global flow appears to be important at higher frequencies for more realistic microstructures (models like pores and randomly oriented cracks or pores, randomly oriented cracks and aligned mesoscopic fractures).

The attenuation peak of squirt flow move towards relatively low frequencies with the increase of viscosity i.e. changing saturating fluid from water to oil, while the global flow attenuation peak move towards relatively high frequencies with the increase of viscosity. The attenuation peak of the global flow obtained using the approximate wave number is always shifted to the right as compared to the solution with correct wave number (exact analytical or iterative solution).

The observations of negative velocity dispersion in Jakobsen and Chapman (2009) theory still remain, even if we use the correct effective wave number, when dealing with the phenomenon of wave-induced fluid flow in models of cracked /fractured porous media where global flow effects dominates.

We may also conclude from these numerical experiments that at seismic frequencies global flow effects are not so important and needs very high permeability and low viscosity to have an effect.

Acknowledgements

PhD student Aamir Ali would like to thank Higher Education Commission (HEC), Pakistan, and Department of Earth Sciences, University of Bergen, Norway, for providing the necessary funding to complete this work.

References

Agersborg R., Jakobsen M., Ruud B.O., and Johansen T.A., 2007. Effects of pore fluid pressure on the seismic response of a fractured carbonate reservoir, *Studia Geophysica et Geodaetica* **51**, 89-118.

Auld, B.A., 1990. Acoustic Fields and Waves in Solids, Krieger Publishing, Malabar, FL.

Biot, M.A., 1956. Theory of propagation of elastic waves in a fuid saturated porous solid. I. Low frequency range and II. Higher-frequency range. *J. Acoust. Soc. Am.,* **28**, 168-191.

Biot, M. A., 1962. Mechanics of deformation and acoustic propagation in porous media, *J. appl. Phys.*, **33**, 1482-1498.

Carcione, J.M., 1995. Constitutive model and wave equations for linear, viscoelastic, anisotropic media, *Geophysics*, **60**, 537–548.

Carcione, J.M., 2007. Wave fields in real media: Wave propagation in anisotropic, anelastic, porous and electromagnetic media: *Elsevier Science Publishing Company, Inc*.

Chapman, M., 2001. Does fluid viscosity influence seismic velocity? 63rd Annual International EAGE Meeting, Amsterdam, The Netherlands, 11 - 15 June.

Chapman, M., V. Zatsepin, S., and Crampin, S., 2002. Derivation of a microstructural poroelastic model, *Geophys. J. Int*., **151**, 427-451.

Chapman, M., 2003. Frequency dependent anisotropy due to meso-scale fractures in the presence of equant porosity, *Geophys. Prosp*., **51**, 369-379.

Dvorkin, J., and Nur, A., 1993. Dynamic peorelasicity: a unified model with the squirt and Biot mechanism, *Geophsyics*, **58**, 524-533.

Dvorkin, J., Nolen-Hoeksema, R., and Nur, A., 1994. The squirt flow mechanism: Macroscopic description, *Geophsyics*, **59**, 428-438.

Dvorkin, J., Mavko, G. and Nur, A., 1995. Squirt flow in fully saturated rocks, *Geophysics*, **60**, 97-109.

Hudson, J.A., Liu, E., and Crampin, S., 1996. The mechanical properties of materials with interconnected cracks and pores, *Geophys. J. Int.*, **124**, 105-112.

Jakobsen, M., Hudson, J.A., and Johansen, T.A., 2003a. T-matrix approach to shale acoustics. *Geophys. J. Int.*, **154**, 533-558.

Jakobsen, M., Johansen, T.A., and McCann, C., 2003b. The acoustic signature of fluid flow in complex porous media, *J. Appl. Geophys.*, **54**, 219-246.

Jakobsen, M., 2004. The interacting inclusion model of wave-induced fluid flow, *Geophys. J. Int.,* **158**, 1168-1176.

Jakobsen, M., 2007. Effective hydraulic properties of fractured reservoirs and composite porous media, *J. Seism. Expl.,* **16**, 199-224.

Jakobsen, M., and Chapman, M., 2009. Unified theory of global and squirt flow in cracked porous media. *Geophysics*, **74**, WA65-WA76.

Mavko, G., and Jizba, D., 1991. Estimating grain-scale fluid effects on velocity dispersion in rocks, *Geophysics,* **56**, 1940-1949.

Mavko, G., and Nur, A., 1975. Melt squirt in the asthenosphere, *J. Geophys. Res.,* **80**, 1444-1448.

Mukerji, T., and Mavko, G., 1994, Pore fluid effects on seismic velocity in anisotropic rocks, *Geophysics*, **59**, 233-244.

O' Connell, R.J., and Budiansky, B., 1977. Viscoelastic properties of fluid-saturated cracked solids, *J. Geophys. Res.,* **82**, 5719-5735.

Pointer, T., Liu, E., and Hudson, J.A., 2000. Seismic wave propagation in cracked porous media, *Geophys. J. Int.,* **142**, 199-231.

Shahraini, A., Ali, A., and Jakobsen, M., 2010. Characterization of fractured reservoirs using a consistent stiffness-permeability model: focus on the effects of fracture aperture, *Geophys. Prospect.,* **59**, 492-505.

Van Golf-Racht, T.D., 1982. Fundamentals of Fractured Reservoirs Engineering, *Elsevier*. ISBN 0444416250.

Winkler, K.W., 1985. Dispersion analysis of velocity and attenuation in Berea sandstone, *J. Geophys. Res.,* **90**, 6793-6800.

Xi, D., Liu, X., and Zhang, G., 2007. The Frequency (or Time) – Temperature Equivalence of Relaxation in Saturated Rocks, *Pure appl. Geophys.,* **164**, 2157-2173.

Appendix-A Christoffel equation for viscoelastic media

From Hooke's law the stress-strain relation can be written as using the matrix notation (Carcione, 2007)

$$\boldsymbol{\sigma} = \mathbf{C} \cdot \mathbf{e} \tag{A-1}$$

where $\boldsymbol{\sigma}$ is the stress tensor, $\mathbf{e}$ is the strain tensor and $\mathbf{C}$ is the stiffness tensor. The equation of motion in the absence of body forces can be written as (Carcione, 2007)

$$\boldsymbol{\Gamma}_{\nabla} \cdot \mathbf{u} = \rho \partial_{tt}^2 \mathbf{u}, \tag{A-2}$$

where

$$\boldsymbol{\Gamma}_{\nabla} = \nabla \cdot \mathbf{C} \cdot \nabla^T, \tag{A-3}$$

where $\mathbf{u}$ is the displacement vector and the symmetric gradient operator ∇ using the matrix representation is given by (Auld, 1990; Carcione, 2007)

$$\nabla = \begin{bmatrix} \partial_1 & 0 & 0 & 0 & \partial_3 & \partial_2 \\ 0 & \partial_2 & 0 & \partial_3 & 0 & \partial_1 \\ 0 & 0 & \partial_3 & \partial_2 & \partial_1 & 0 \end{bmatrix}. \tag{A-4}$$

The strain displacement relation is given by (Carcione, 2007)

$$\mathbf{e} = \nabla^T \cdot \mathbf{u}. \tag{A-5}$$

A general plane wave solution for the displacement vector of the body waves is given by (Carcione, 2007)

$$\mathbf{u} = \mathbf{u}_0 \exp\left[i(\omega t - \mathbf{k} \cdot \mathbf{x})\right], \tag{A-6}$$

where $\mathbf{u}_0$ represents a constant complex vector, ω is the angular frequency and $\mathbf{k}$ is the wave-number vector. The particle velocity is given by time derivative of equation (A-6) given by

$$\mathbf{v} = \partial_t \mathbf{u} = i\omega \mathbf{u}. \tag{A-7}$$

In the absence of body forces $(\mathbf{f} = 0)$, we consider plane waves propagating along the direction given by (Carcione, 2007)

$$\hat{\mathbf{k}} = l_1\hat{\mathbf{e}}_1 + l_2\hat{\mathbf{e}}_2 + l_3\hat{\mathbf{e}}_3\,, \tag{A-8}$$

where l_1, l_1 and l_1 are the direction cosines. The wave-number vector $\mathbf{k}$ can be written as (Carcione, 2007)

$$\mathbf{k} = (k_1, k_2, k_3) = k(l_1, l_2, l_3) = k\hat{\mathbf{k}}, \tag{A-9}$$

where k is the magnitude of the wave-number vector. The spatial differential operator in equation (A-4) can be replaced by

$$\nabla \rightarrow -ik\begin{bmatrix} l_1 & 0 & 0 & 0 & l_3 & l_2 \\ 0 & l_2 & 0 & l_3 & 0 & l_1 \\ 0 & 0 & l_3 & l_2 & l_1 & 0 \end{bmatrix} \equiv -ik\mathbf{L}. \tag{A-10}$$

Now substituting the time derivative as $\partial_t \rightarrow i\omega$ and using equation (A-10) in equation (A-2), we get (Carcione, 2007)

$$k^2\boldsymbol{\Gamma}\cdot\mathbf{u} = \rho\omega^2\mathbf{u}, \tag{A-11}$$

where

$$\boldsymbol{\Gamma} = \mathbf{L}\cdot\mathbf{C}\cdot\mathbf{L}^T\,, \tag{A-12}$$

is the Christoffel matrix. The dispersion relation is given by (Carcione, 2007)

$$\det(\boldsymbol{\Gamma} - \rho V^2\mathbf{I}_3) = 0. \tag{A-13}$$

where

$$V = \frac{\omega}{k}\,, \tag{A-14}$$

is the complex velocity.

The equation (A-13) is known as the Christoffel equation. Using equation (A-14), the components of the slowness and attenuation vectors can be expressed in terms of the complex velocity as (given by Carcione, 1995)

$$\mathbf{s} = \mathrm{Re}\left[\frac{1}{V}\right]\hat{\mathbf{k}}\,, \tag{A-15}$$

and

$$\alpha = -\omega\,\mathrm{Im}\left[\frac{1}{V}\right]\hat{\mathbf{k}}. \tag{A-16}$$

Appendix-B The effective permeability tensor

The effective permeability tensor $\mathbf{K}^*$ of the fractured porous reservoir model, assuming that the distribution of fractures is same for all fracture families is given by (Jakobsen 2007)

$$\mathbf{K}^* = \mathbf{K}^{(0)} + \mathbf{K}_1 \cdot (\mathbf{I}_2 + \mathbf{g}_d \cdot \mathbf{K}_1)^{-1}, \tag{B-1}$$

where

$$\mathbf{K}_1 = \sum_r v^{(r)} \boldsymbol{\tau}^{(r)}. \tag{B-2}$$

Here, $\mathbf{K}^{(0)}$ is background or matrix permeability, $\mathbf{I}_2$ is the (Kronecker-delta) identity for second rank tensors, $v^{(r)}$ is the volume concentration for fractures of type r and $\mathbf{g}_d$ is a tensor given by the strain Green's function integrated over an ellipsoid determining the symmetry of the correlation function for the spatial distribution of fractures (see Jakobsen 2007, Shahraini *et al*. 2010). The $\boldsymbol{\tau}^{(r)}$ for a single fracture of type r is given by (Jakobsen 2007)

$$\boldsymbol{\tau}^{(r)} = (\mathbf{K}^{(r)} - \mathbf{K}^{(0)}) \cdot \left[\mathbf{I}_2 - \mathbf{g}^{(r)} \cdot (\mathbf{K}^{(r)} - \mathbf{K}^{(0)})\right]^{-1}. \tag{B-3}$$

Here, $\mathbf{g}^{(r)}$ is a second-rank tensor given by the pressure gradient Green's function integrated over a characteristic spheroid having the same shape as inclusions of type r (see Jakobsen 2007, Shahraini *et al*. 2010), and $\mathbf{K}^{(r)}$ is a second-rank tensor of permeability coefficients for fractures of type r, which can be estimated using the cubic law given by (Van Golf-Racht 1982)

$$\mathbf{K}^{(r)} = \frac{(a^{(r)})^2}{12} \mathbf{I}_2. \tag{B-4}$$

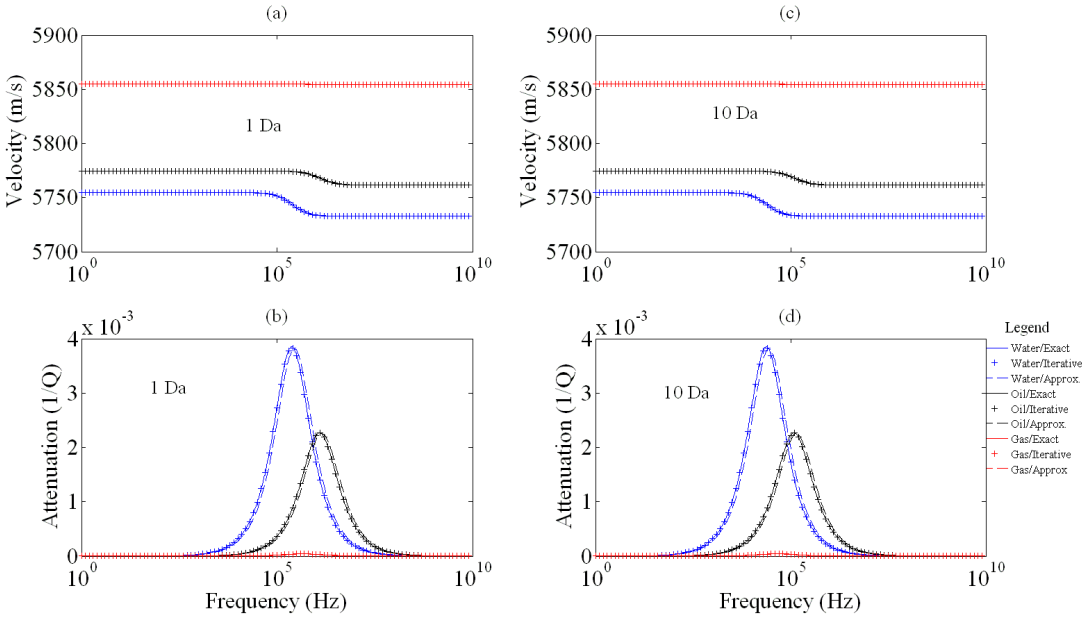

Figure 1. Spherical pores - First-order T-matrix estimates of velocity and attenuation spectra for different fluid mobilities. The exact, iterative and approximate solutions are presented. The porosity of spherical pores is 10%. Panels (a) and (b) show results with permeability of 1 Darcy. Panels (c) and (d) show the same as panels (a) and (b) but with permeability of 10 Darcy.

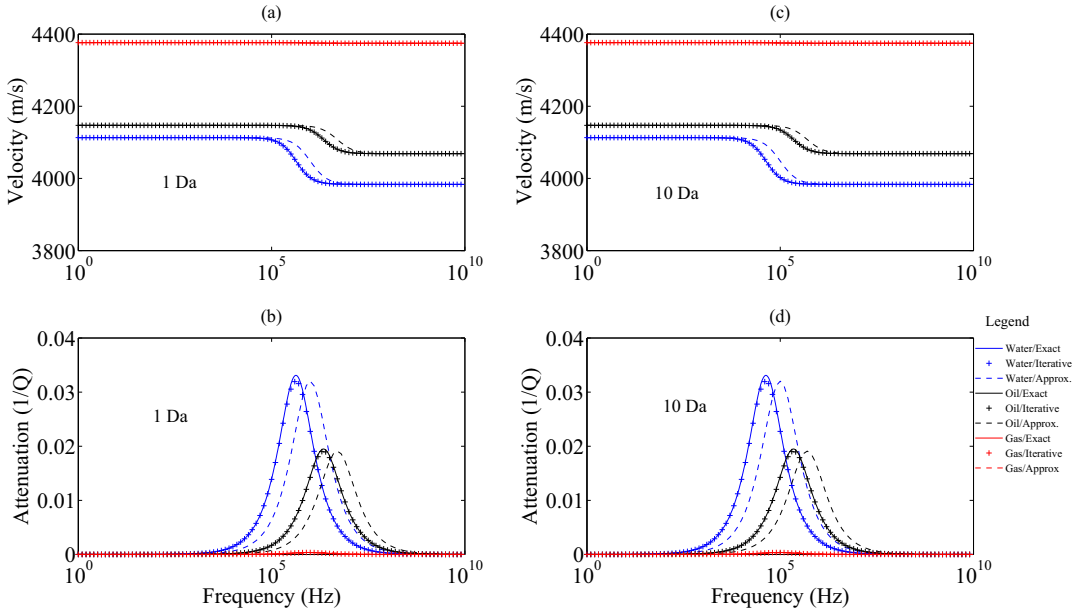

Figure 2 Same as Fig.1, but the porosity of spherical pores is 35%.

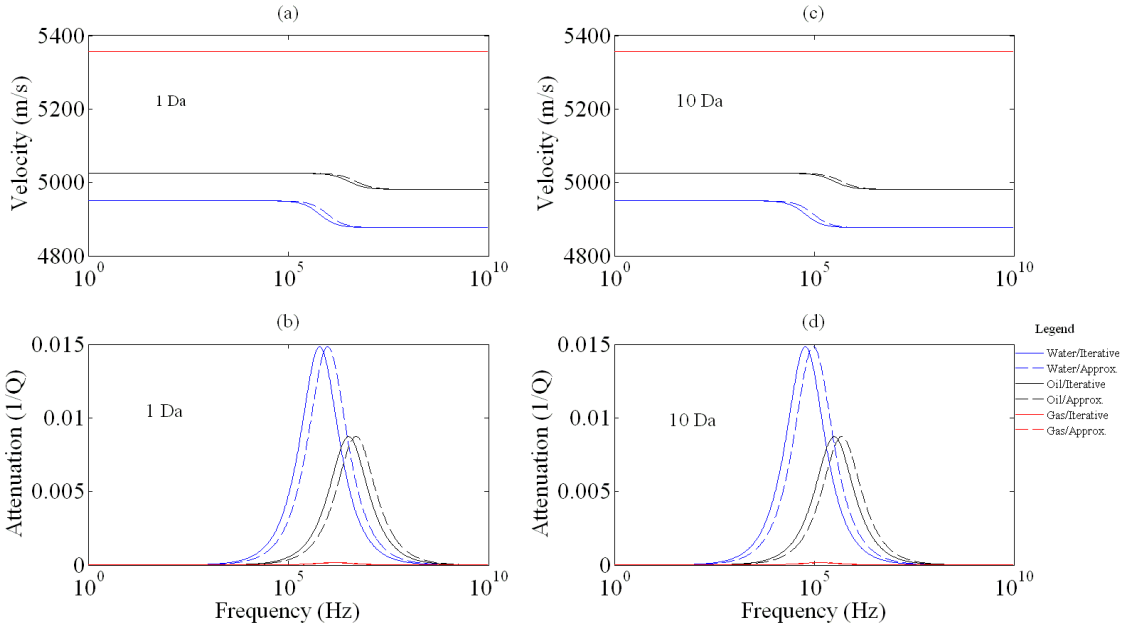

Figure 3. Spherical pores - Higher-order T-matrix estimates of velocity and attenuation spectra for different fluid mobilities. The iterative and approximate solutions are presented. The porosity of spherical pores is 35%.

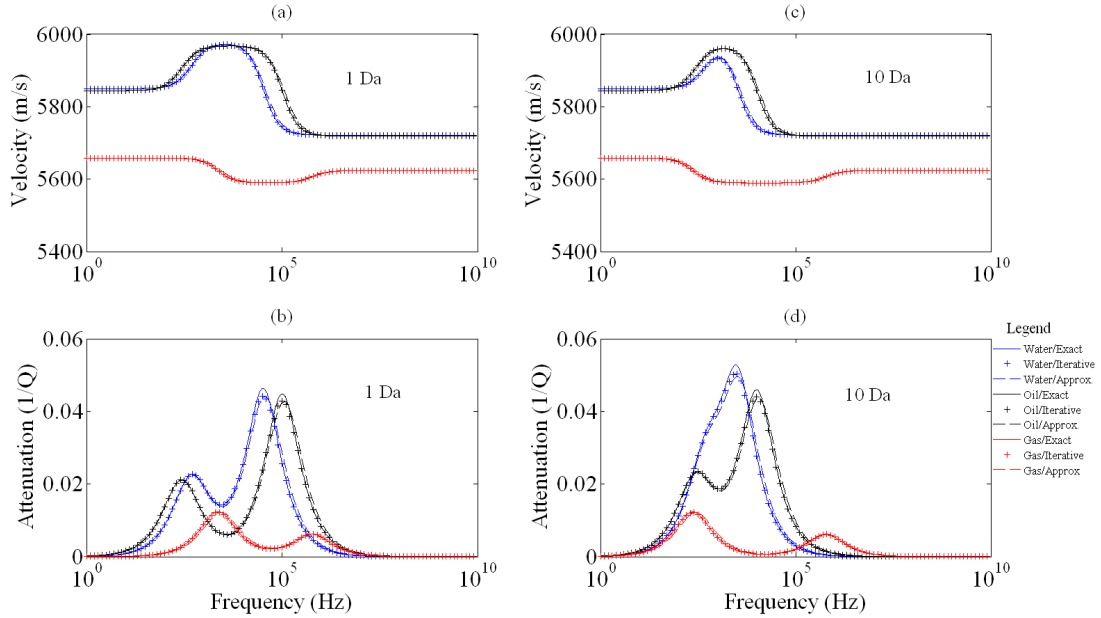

Figure 4. Randomly oriented micro-cracks - First-order T-matrix estimates of velocity and attenuation spectra for different fluid mobilities. The exact, iterative and approximate solutions are presented. The aspect ratio of randomly oriented cracks is 1/1000, while crack density is 0.1. Panels (a) and (b) show results with permeability of 1 Darcy. Panels (c) and (d) show the same as panels (a) and (b) but with permeability of 10 Darcy.

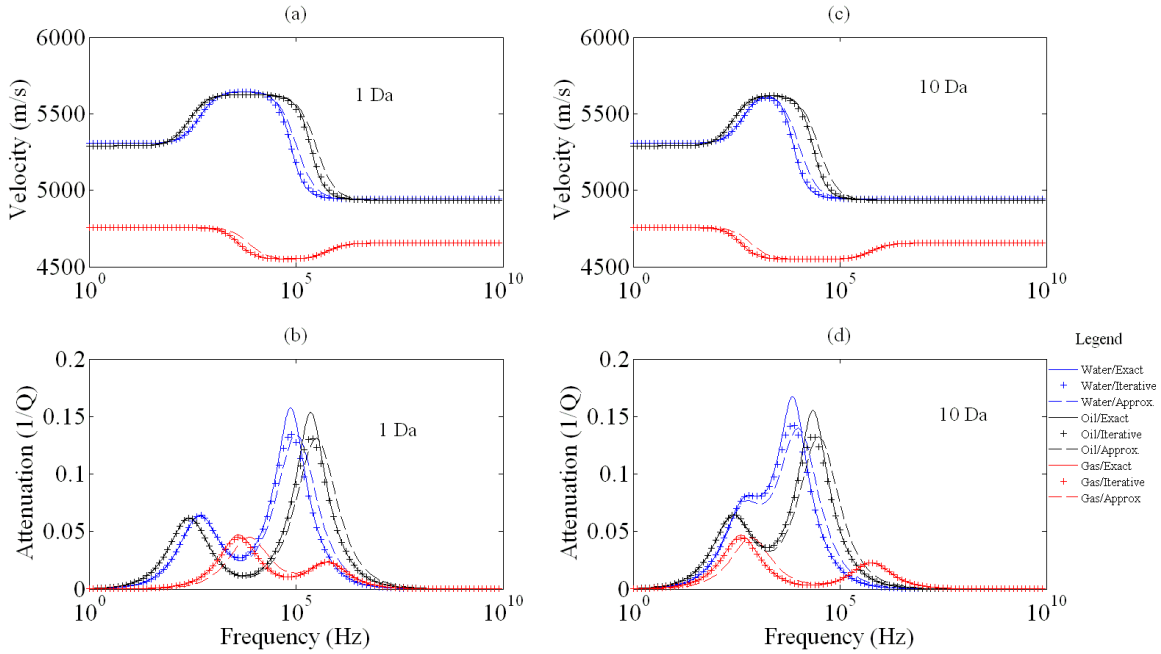

Figure 5. Same as Fig.4, but the crack density was 0.25.

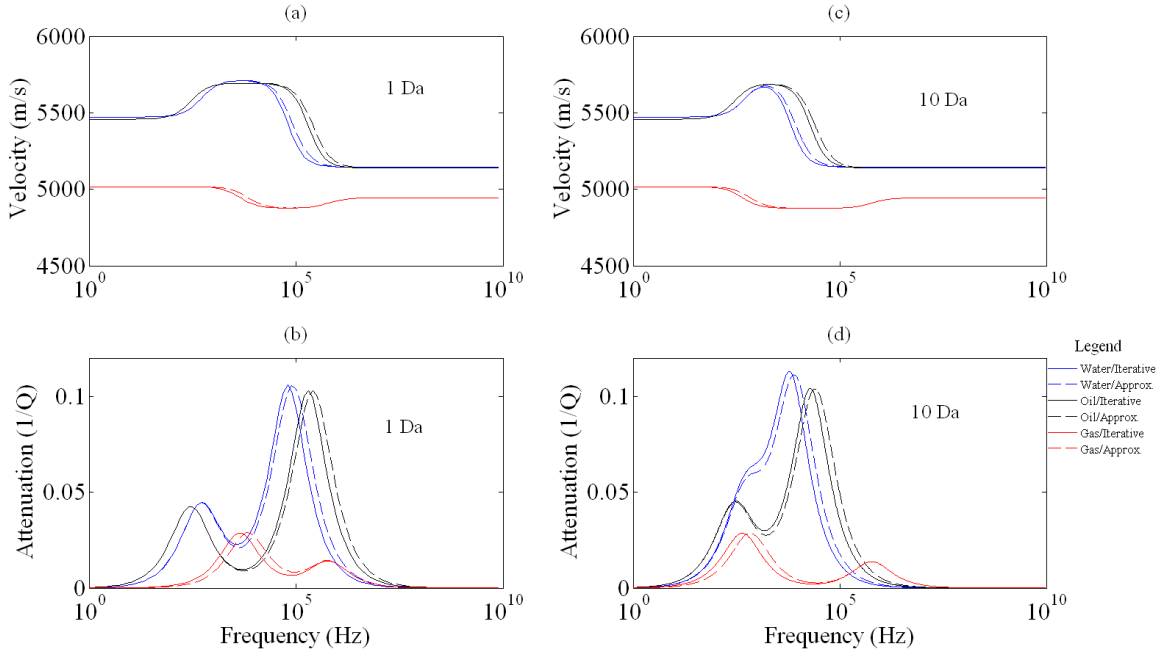

Figure 6. Randomly oriented micro-cracks - Higher-order T-matrix estimates of velocity and attenuation spectra for different fluid mobilities. The iterative and approximate solutions are presented. The aspect ratio of randomly oriented cracks is 1/1000, while crack density is 0.25.

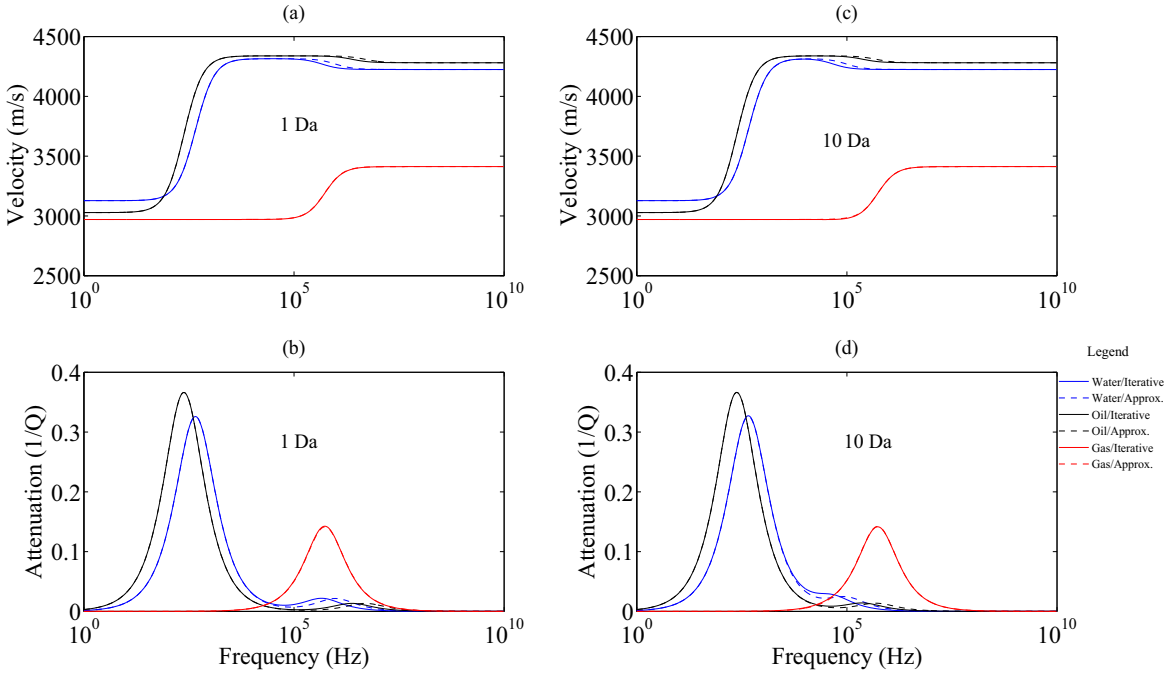

Figure 7. Pores and randomly oriented micro-cracks - Higher-order T-matrix estimates of velocity and attenuation spectra for different fluid mobilities. The iterative and approximate solutions are presented. The aspect ratio of randomly oriented micro-cracks is 1/1000. The porosity and crack density is 35% and 0.4, respectively. Panels (a) and (b) show results with permeability of 1 Darcy. Panels (c) and (d) show the same as panels (a) and (b) but with permeability of 10 Darcy.

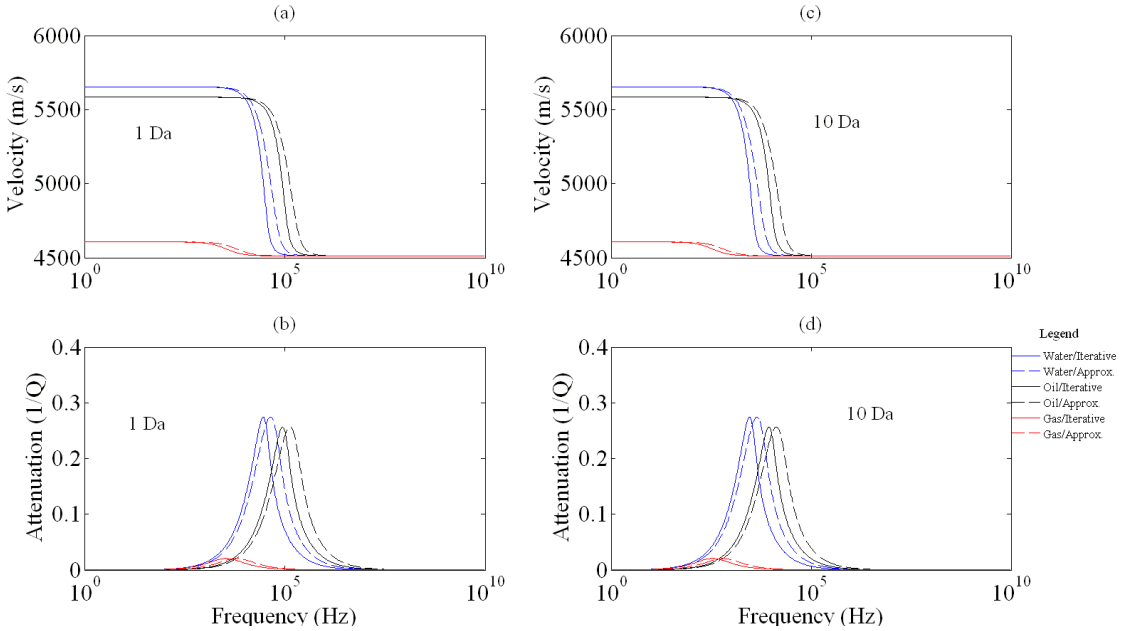

Figure 8. Aligned micro-cracks - Higher-order T-matrix estimates of velocity and attenuation spectra for the plane wave propagation with polar and azimuthal angles of 30° and 45° for different fluid mobilities. The iterative and approximate solutions are presented. The crack density of aligned micro-cracks is 0.3. Panels (a) and (b) show results with permeability of 1 Darcy. Panels (c) and (d) show the same as panels (a) and (b) but with permeability of 10 Darcy.

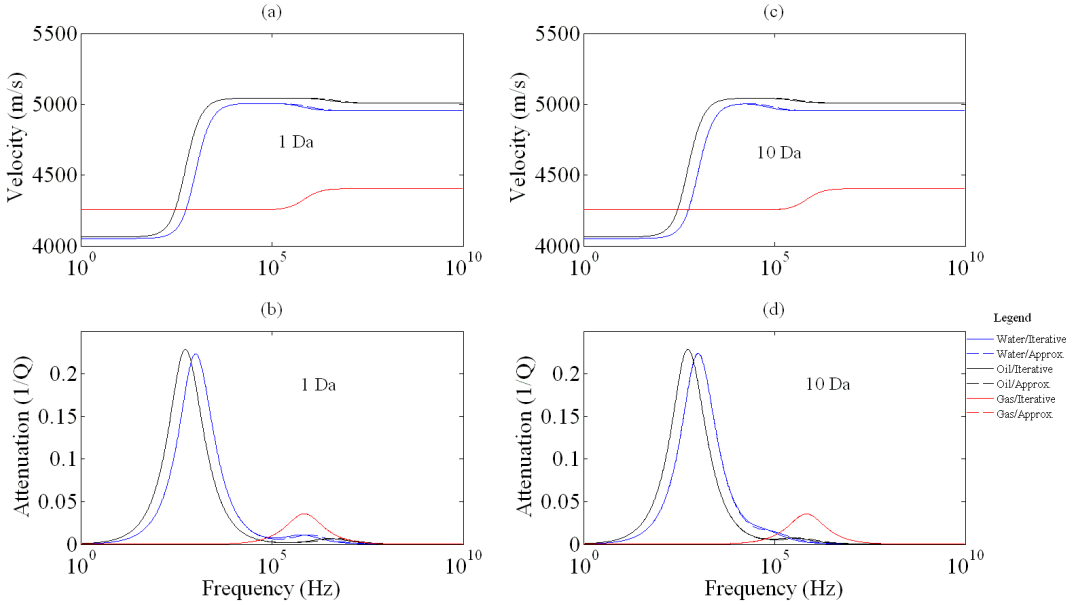

Figure 9. Pores and aligned micro-cracks - Higher-order T-matrix estimates of velocity and attenuation spectra for the plane wave propagation with polar and azimuthal angles of 30° and 45° for different fluid mobilities. The aspect ratio of aligned micro-cracks is 1/1000. The porosity and crack density is 35% and 0.4, respectively. Panels (a) and (b) show results with permeability of 1 Darcy. Panels (c) and (d) show the same as panels (a) and (b), but for a permeability of 10 Darcy.

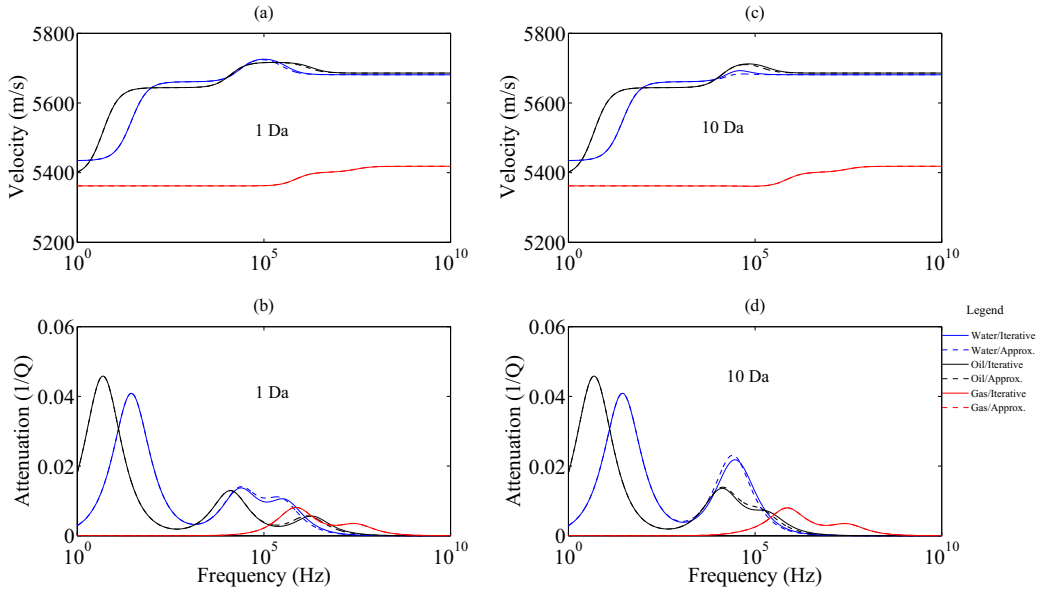

Figure 10. Pores, randomly oriented micro-cracks and meso-fractures - Higher-order T-matrix estimates of velocity and attenuation spectra for the plane wave propagation with polar and azimuthal angles of 30° and 45° for different fluid mobilities. The aspect ratio of randomly oriented micro-cracks and aligned meso-fracture set is 1/1000. The porosity (spherical pores), crack density (randomly oriented cracks) and fracture density (aligned set of mesoscopic fractures) is 10%, 0.01 and 0.4, respectively. Panels (a) and (b) show results with permeability of 1 Darcy. Panels (c) and (d) show the same as panels (a) and (b), but for a permeability of 10 Darcy.